Comparison of Respirable Coal Mine Dust Constituents Estimated using FTIR, TGA, and SEM–EDX

Nishan Pokhrel[1] · **Eleftheria Agioutanti**[1] · **Cigdem Keles**[1] · **Setareh Afrouz**[1] · **Emily Sarver**[1]

Abstract

Since the mid-1990s, there has been a resurgence of severe lung disease among US coal miners. This has prompted efforts to better characterize and monitor respirable dust exposures—especially with respect to mineral constituents sourced from rock strata surrounding the coal, which is believed to play a central role in many cases of disease. Recently, a rapid analysis method for silica (quartz) mass has been developed using direct-on-filter Fourier transform infrared (FTIR) spectroscopy. It can concurrently provide an estimate of kaolinite, presumably a primary silicate mineral in many coal mines. Other methods, including thermogravimetric analysis (TGA) and scanning electron microscopy with energy-dispersive X-ray (SEM–EDX), can also be used to estimate respirable coal mine dust constituents. However, there have been few efforts to compare results across multiple methods. Here, FTIR, TGA, and SEM–EDX were used to analyze 93 sets of respirable dust samples collected in 16 underground coal mines across the USA.

1 Introduction

Exposure to respirable dust has long been recognized as an occupational health hazard to coal mine workers [1, 2]. Respirable crystalline silica (RCS) contained in the dust can be particularly hazardous [3–5]. Indeed, RCS has been cited as a causal factor in a dramatic resurgence of severe and rapid lung diseases among coal miners in central Appalachia over the past two decades [6–8]. This has renewed efforts to improve RCS monitoring in coal mines [9–11]. Moreover, based on knowledge gaps surrounding the whole composition of respirable coal mine dust, and its variability with different geologic and mining conditions, there have been calls to better characterize the dust in general [2].

Traditionally, measurement of silica in US coal mines is taken using the MSHA P7 Standard Method [12]. It uses infrared spectroscopy (IR) to analyze the quartz mass in a dust sample, following the ashing of the sample filter. (It is noted that quartz is well established as the primary form of crystalline silica in coal mine environments, and the terms quartz and silica are often used interchangeably.) However, because of the

sample preparation and equipment required for the P7 analysis, it is practically limited to centralized laboratories. This translates to considerable lag time (days to weeks) between sample collection and reporting of results—which impedes swift mitigation of hazardous exposure conditions [10, 13].

To address this issue, the US National Institute for Occupational Safety and Health (NIOSH) has been working to develop a new direct-on-filter (DOF) approach for quartz measurement [10, 11, 13, 14]. Like Method P7, this method analyzes the quartz in a filter sample. While it is not a real-time measurement, it requires no sample preparation and uses a portable Fourier transform infrared (FTIR) instrument, such that the analysis can be done immediately after sample collection. Miller et al. found strong linear correlations (ranging from 0.90 to 0.97) between DOF and P7-derived quartz data, demonstrating its potential as an end-of-shift method [13].

Although the primary focus of the DOF-FTIR method has been on quartz measurement, it has the potential to provide broader insights into the range of mineral constituents that make up respirable coal mine dust [10, 14]. Similar to the determination of quartz from its characteristic peaks in the FTIR spectrum, other minerals can also be identified and possibly quantified from the spectrum. In fact, kaolinite, which is generally expected to be one of the predominant silicate minerals in many coal mine environments [5, 15], is already an integral part of the quartz quantification method; kaolinite has an overlapping peak with quartz, and

✉ Nishan Pokhrel
nishan@vt.edu

✉ Emily Sarver
esarver@vt.edu

1 Virginia Polytechnic Institute and State University, Blacksburg, VA, USA

Table 1 Comparable constituents across each of the three methods

	Comparison of constituents attributed to likely sources				
Method	Rock strata			Rock dust products	Coal strata
FTIR	Q	K	$Q + K$	-	-
TGA	-	-	Non-carbonate minerals	carbonates	coal
SEM–EDX	S	ASK	$S + ASK + ASO + SLO + M$	CB	$C + MC$

this interference is quantified (in terms of spectrum peak area) in order to analytically correct the quartz measurement [10, 13, 16]. Thus, kaolinite mass (K), along with quartz (Q), can be easily reported from the DOF-FTIR analysis of coal mine dust samples using calibration curves for each analyte. It is possible to estimate the mass of other minerals of interest too (e.g., calcite, which has been the focus of a separate study on the contribution of limestone rock dusting products to respirable coal mine dust [17]). Additionally, Stach et al. explored the development of an alternative analytical method (that combines transmission and diffuse reflection FTIR) to quantify alpha quartz, dolomite, and calcite in respirable mine dust samples [18].

In addition to FTIR, other analytical methods can also be used to characterize respirable coal mine dust. Thermogravimetric analysis (TGA) is a mass-based method that can be applied to determine coal, non-carbonate minerals, and carbonates fractions of dust, which can be loosely associated with dust sources related to coal cutting, rock strata cutting/drilling, and rock dust application, respectively, in many mines [19]. TGA basically tracks the weight change of a sample with temperature in a controlled environment. Since coal, carbonates, and non-carbonates have their own thermal behavior (i.e., coal and carbonates tend to lose mass in characteristic temperature regions, while the non-carbonate minerals of interest like silica and silicates tend to be inert in those regions), the sample behavior can be used to estimate these three primary fractions [19]. Further, if rock-strata sourced dust in a coal mine is dominated by silica and silicates, the non-carbonate minerals fraction might be comparable to the $Q + K$ per the FTIR (Table 1).

Scanning electron microscopy with energy-dispersive X-ray (SEM–EDX) analysis is a particle-based method that can be used to size and classify individual particles. For respirable coal mine dust, the authors' group has established routines to bin particles into the following predefined mineralogy classes: carbonaceous (C) and mixed carbonaceous (MC), which are generally associated with coal dust and/or diesel particulates (in the very fine sizes); aluminosilicates (AS, which can be further sub-classified as either kaolinite ASK, or other aluminosilicates, ASO), other silicates (SLO), silica (S), and metal oxides and sulfides (M), which are generally associated with rock-strata sourced dust; carbonates (CB), which are associated with rock dust (e.g., limestone) application in most US mines; and others (O), which are particles

not otherwise classified [20–22]. It stands to reason that the distribution of dust across these classes might also be comparable to FTIR and TGA measures per Table 1.

Though FTIR, TGA, and SEM–EDX can all be applied to respirable coal mine dust, they have heretofore not been used together or directly compared. These were the primary aims of the study reported here.[1]

2 Materials and Methods

2.1 Sample Collection

Respirable dust samples were collected in 2018 from 16 different US underground coal mines (numbered 10–25), representing five mine regions: northern Appalachia (NA, mines 7–9), central Appalachia (CA, mines 10–15, 21, 22, 25), western coal basin (W, mines 23 and 24), and mid-western Illinois coal basin (MW, mines 19 and 20) [21]. A total of 93 sets of samples (each containing multiple replicates) were collected in several key locations in each mine: near the coal 'feeder (F)' or along the main conveyor belt, near the 'intake (I)' (including near the headgate of a longwall); near major 'production (P)' activities (i.e., downwind of a continuous miner or along the longwall face); in the 'bolter (B)' (i.e., just downwind of an active roof-bolter); and in the 'return (R)' (including near the tailgate of a longwall). Each sample set was collected over about 2–4 h.

Escort ELF air sampling pumps with a 10-mm nylon Dorr-Oliver cyclone at a flow rate of 2.0 LPM (yielding a d50 of about 3.5 µm) were used to collect dust onto 37-mm filters in two-piece styrene cassettes. For the FTIR analysis, the samples were collected onto polyvinyl chloride filters

---

(PVC, 5.0 μm pore size), while for SEM and TGA, polycarbonate filters (PC, 0.4 μm pore size) were used [19, 22, 23]. The PVC filters were pre- and post-weighed using a microbalance (Sartorius MSE6.6S, Gottingen, Germany) to determine the total dust mass.

2.2 FTIR Analysis

For each sample set, one PVC filter was prepared for analysis by an ALPHA II FTIR Spectrometer (Bruker Optics, Billerica, MA) to get the absorbance spectra between spatial frequencies of 4000 cm^{-1} to 400 cm^{-1}. The PVC filters were carefully taken out from the 2-piece cassettes and placed onto FTIR-compatible 4-piece cassettes (Zefon International, Ocala, FL), which were then mounted centrally onto a sample holder within the chamber of the FTIR instrument [24]. Sixteen scans of the center 6-mm-diameter spot on each filter were taken at a resolution of 4 cm^{-1} using Blackman-Harris three-term apodization, which then underwent a rubber band baseline correction with 64 baseline points (to remove distortions) [13, 14].

Being a direct-on-filter approach, the FTIR spectra obtained on a dust sample also include the absorbance data of the filter material. This was addressed by subtracting the background spectrum of a blank PVC filter. Blank filter data were obtained for each batch of dust samples analyzed by FTIR to ensure that any effect of environmental conditions (e.g., humidity) was minimized.

In an absorbance spectrum for a pure sample, quartz appears as a doublet peak at 780 and 800 cm^{-1}, while kaolinite appears as a larger peak at 915 cm^{-1} and a smaller peak at 790 cm^{-1}. Using Bruker's OPUS software (version 8.2.28, 32 bit), the spectral region between 816 and 767 cm^{-1} (corresponding to the doublet peak for Q) and between 930 and 900 cm^{-1} (corresponding to the larger peak for K) was integrated to find the peak areas, using calculations consistent with other IR methods for quartz analysis [12, 13]. Since the smaller peak of K lies in the same range for quartz doublet peak, the Q peak area was corrected for this interference using a previously calculated correction ratio of 3.8 for the FTIR instrument [13, 14]. This was done using the following equation [13]:

$$Corrected\ Q\ peak\ area = Q\ peak\ area - \frac{K\ peak\ area}{3.8}$$

These peak areas of the 6-mm spot on the filter center were extrapolated to determine the total Q and K masses on the entire 37-mm filter. This was done using previously established calibration curves developed by NIOSH from regression analysis of the peak integrated area versus the gravimetric mass of pure crystalline silica (Min-U-Sil 5), kaolinite, or a mixture of the two aerosolized in a calm-air laboratory dust chamber [10, 14, 25]. It is important to note that those calibration curves were developed with samples collected in 3-piece cassettes (again using 10-mm nylon Dorr-Oliver cyclones at 2 LPM flow rate). Since the mine samples used in this study were collected in 2-piece cassettes—which promote a slightly different dust loading pattern—the FTIR-derived Q and K mass results were also corrected using a previously established correction factor of 0.877 [11]. Finally, the quantified masses were converted to mass percentages using total mass of the samples.

2.3 TGA Analysis

One PC filter from each sample set was used for TGA per Agioutanti et al. [19]. Briefly, dust was recovered from the sample filters by sonication in isopropanol, redeposited in a clean, tared sample pan, and analyzed by a Q500 Thermogravimetric Analyzer (TA Instruments, New Castle, DE) using the prescribed thermal ramping routine. (Notably, the same instrument used by Agioutanti et al. was used here.) Agioutanti et al. showed that weight change in several regions of interest could be used to estimate the coal, carbonates, and non-carbonate mineral mass fractions in the sample and published a series of mass balance equations that can be applied to a sample thermogram for this purpose [19]. These were applied to all sample thermograms here.

2.4 SEM–EDX Analysis

Finally, one PC filter from each sample set was also analyzed by SEM–EDX. Dust samples were prepared and particles (1–10 μm) analyzed based on the method described by Sarver et al. [21], with a computer-controlled routine using an FEI Quanta 600 FEG environmental scanning electron microscope (ESEM) (Hillsboro, OR, USA) equipped with a backscatter electron detector (BSD) and a Bruker Quantax 400 EDX spectroscope (Ewing, NJ, USA). Using Bruker's Esprit software (version 1.9.4), the routine scanned multiple areas across each sample in order to analyze about 500 particles per sample. For each particle, the long and intermediate dimensions and projected area were recorded, and its elemental spectra were used to classify its mineralogy (Table 2). These data were then used to estimate the particle's mass. The volume was calculated as the product of the projected area and estimated thickness (i.e., an assumed value for the particle's short dimension; assumptions for short-to-intermediate dimension ratio (SI) and specific gravity (SG) are shown in Table 2 for each class. Computed particle masses in each class were summed and divided by the total particle mass for the sample to estimate the mass fraction (%) for each class, which were then compared to the FTIR and TGA results.

Table 2 SEM–EDX classification criteria for supramicron particles, along with assumptions for S:I ratio and SG for each mineralogy class (adapted from [21])

Class	Atomic %								Particle size to mass assumptions	
	O	Al	Si	C	Mg	Ca	Ti	Fe	SI	SG
C	< 29	≤ 0.3	≤ 0.3	≥ 75	≤ 0.5	≤ 0.41	≤ 0.06	≤ 0.15	0.6	1.4
MC		≤ 0.35	< 0.35		≤ 0.5	≤ 0.5	≤ 0.6	≤ 0.6	0.6	1.4
ASK[1]		≥ 0.35 (≥ 39)	≥ 0.35 (≥ 32)		(< 15)	(< 8)	(< 13)	(< 13)	0.4	2.6
ASO[1]		≥ 0.35 (< 39)	> 0.35 (< 32)		(≥ 15)	(≥ 8)	(≥ 13)	(≥ 13)	0.4	2.6
SLO[2]			≥ 0.33						0.4	2.6
S[3]			≥ 0.33						0.7	2.65
M		> 1					> 1	> 1	0.7	4.96
CB	> 9				> 0.5	> 0.5			0.7	2.7

[1]To differentiate ASK from ASO, additional limits for Al, Si, Mg, Ca, Ti and Fe are shown in parenthesis (normalized to exclude C and O)

[2]Additional limits for SLO: $Si/(Al+Si+Mg+Ca+Ti+Fe) < 0.5$

[3]Additional limits for S: $Al/Si < 1/3$ and $Si/(Al+Si+Mg+Ca+Ti+Fe) \geq 0.5$

3 Results and Discussion

Table 3 summarizes the FTIR, TGA, and SEM–EDX results from all 93 sets of respirable mine dust samples included in the study. (The data presented in the table are substantially the same as reported in [26], slight changes in FTIR-K values are related to application of an improved integrated peak area to mass calibration curve.) It is noted that the TGA recovered mass refers to the sum of the coal, carbonates, and non-carbonate mineral masses determined for each PC sample analyzed. However, this may not match the total sample mass for the paired PVC filter due to several factors including differences in total mass collected on each filter (i.e., due to differences in the filter media themselves or spatial variation in the sampling environment) and less than 100% recovery of dust from the PC filter. That said, PVC sample mass and TGA recovered mass do generally trend together.

The sample mass (determined from the PVC filters in each set) was generally highest in the P and R sampling locations (mean values of 0.75 and 1 mg, respectively), while masses in the I, B, and F locations were lower (means of 0.2, 0.3, and 0.3 mg, respectively). It is worth noting that sample masses reported here should not be used as a proxy for mass concentration in the sampling location since the sampling time varied. However, the sample mass does have important ramifications for each analytical method. For SEM–EDX, high-mass samples may exhibit dense loading on the filter, which can challenge the analysis of individual particles. Though no mass limit has been established, care was taken to avoid analysis on filter areas that may have had overlapping particles. Even so, it is possible that elemental spectra on some particles were influenced by surrounding particles.

For TGA, Agioutanti et al. [19] found that limits of detection (LOD) and quantification (LOQ) in lab-generated respirable dust samples were on the order of 50 and 150 µg, respectively, of recovered dust for each primary sample component (i.e., coal, carbonate, or non-carbonates). In real mine dust samples, it is impossible to know the component masses a priori—rather only the total recovered dust mass is known. Given that the current study represents the first time this TGA method has been used for mine dust samples, LOD and LOQ were not applied strictly here. However, results for particularly low-mass samples should be considered with some caution. (For example, using a threshold of 200 µg total recovered dust, about 40 samples per Table 3 would be considered low mass).

Similarly, FTIR results can also be affected by sample mass, and only the total dust mass (on PVC filter) is known a priori. Per Cauda et al. [10], the LOD and LOQ for Q are 5 and 16 µg, respectively, using the same approach to compute LOD and LOQ, the values for K were estimated as ∼ 5 and ∼ 18 µg, respectively. As shown in Table 3, only 27 of the 93 samples had quantifiable Q, with 5 samples between LOD and LOQ, and the rest of them were below LOD (and had total sample mass < 350 µg). In contrast, 64 of the samples had quantifiable K, and the rest were between LOD and LOQ, with the exception of one sample below LOD.

In summary, higher constituent masses are needed to surpass LOD/LOQ for TGA and FTIR, and thus, higher total sample mass is favorable here. On the other hand, a lower sample mass is more favorable for SEM–EDX. The relative agreement between results from each method as a function of sample mass can shed more light on these issues and the design of sampling campaigns.

Table 3 Summary of results for 93 sets of respirable coal mine dust samples (updated from [26])

Sample No.	Mine Region	No.	Sampling location	PVC sample mass (mg)	TGA recovered mass (mg)	FTIR (mass %) Q	K	TGA (mass %) Coal	Carb	Non-carb	SEM–EDX (mass %) C	MC	ASK	ASO	S	SLO	M	CB
1	SCA	10	B	0.148	0.146		28.2	25.4	3.7	70.9	17.8	16.6	25.7	32.7	5.6	0.0	0.8	0.8
2	SCA	10	B	0.181	0.198		30.1	26.8	5.5	67.7	3.8	8.9	47.1	35.3	3.7	0.0	0.3	1.0
3	SCA	10	F	0.132	0.157		26.9	41.7	3.5	54.8	11.3	7.9	32.3	35.3	8.3	0.0	3.9	0.9
4	SCA	10	F	0.183	0.064		20.9	43.6	16.8	39.6	8.3	7.7	37.0	44.2	1.0	0.0	2.0	0.0
5	SCA	10	I	0.005	0.049		n/a*	84.4	1.8	13.7	22.6	14.0	5.4	9.1	41.0	1.3	0.4	6.2
6	SCA	10	P	0.089	n/a		34.1	n/a	n/a	n/a	n/a	n/a	n/a	n/a	n/a	n/a	n/a	n/a
7	SCA	10	P	1.494	1.286		24.3	22.7	3.2	74.1	0.0	0.0	83.5	15.8	0.7	0.0	0.0	0.0
8	SCA	10	R	0.038	0.074		43.5*	62.3	3.3	34.4	28.0	13.2	23.8	24.9	8.3	0.2	0.3	1.3
9	SCA	11	B	0.106	0.042		27.8	36.0	9.3	54.7	1.2	5.2	11.8	60.4	14.2	0.2	1.2	5.8
10	SCA	11	F	0.164	0.104		16.2	54.4	6.9	38.7	23.5	10.8	11.2	30.0	11.1	0.0	7.8	5.6
11	SCA	11	P	1.153	0.666	6.2	13.6	11.4	4.9	83.7	0.0	0.1	3.8	95.4	0.8	0.0	0.0	0.0
12	SCA	11	R	0.749	0.137	6.7	15.9	25.8	5.2	69.0	0.0	0.0	1.8	97.5	0.7	0.0	0.0	0.0
13	SCA	12	B	0.103	0.031		24.0	55.1	13.4	31.4	32.1	16.5	9.7	19.0	4.2	1.0	1.4	16.1
14	SCA	12	I	0.054	0.074		40.3	76.0	5.4	18.6	56.7	8.2	7.0	11.7	5.3	0.0	0.0	11.1
15	SCA	12	P	1.077	0.486	4.0	14.6	29.5	4.8	65.6	7.0	7.5	29.6	52.0	3.4	0.0	0.4	0.0
16	SCA	12	R	0.649	0.430	3.2	17.5	20.8	7.4	71.7	0.1	0.6	7.2	91.3	0.7	0.0	0.0	0.1
17	SCA	13	B	2.535	3.405	12.3	11.5	13.6	5.8	80.6	0.0	0.0	2.1	96.8	1.1	0.0	0.0	0.0
18	SCA	13	F	0.189	0.057		9.6*	78.0	8.1	14.0	36.1	8.4	2.1	7.6	1.1	2.2	1.2	41.2
19	SCA	13	I	0.035	0.030		49.3*	39.9	26.8	33.3	6.5	1.0	1.3	5.7	1.4	0.1	0.0	84.1
20	SCA	13	I	0.701	0.125	4.6	6.7	62.9	12.8	24.4	23.1	10.5	3.7	41.3	7.0	0.0	0.3	14.0
21	SCA	13	R	7.347	11.346	4.7	1.7	8.1	69.5	22.4	0.0	0.0	0.0	9.5	0.0	5.4	0.0	85.0
22	SCA	13	R	1.297	1.312	1.8	3.0	73.9	4.4	21.7	58.9	10.8	5.4	15.4	4.1	0.0	0.1	5.4
23	SCA	14	B	0.039	0.055		48.8*	29.0	12.5	58.6	10.5	6.9	27.9	32.2	16.6	0.0	2.6	3.2
24	SCA	14	F	0.187	0.213		21.8	27.5	5.1	67.4	2.3	4.5	10.6	53.3	13.2	2.1	1.4	12.7
25	SCA	14	I	0.002	0.055		n/a*	66.7	9.2	24.1	8.6	3.8	4.3	16.8	8.7	0.0	0.0	57.9
26	SCA	14	P	4.348	3.682	7.3	12.9	9.5	4.7	85.8	0.0	0.0	2.0	97.9	0.1	0.0	0.0	0.0
27	SCA	21	B	0.085	0.029		23.4*	46.5	10.2	43.3	4.7	8.4	7.9	37.2	15.1	0.1	1.2	25.4
28	SCA	21	F	0.089	0.030		24.0	15.8	2.8	81.5	6.3	10.1	15.9	47.9	11.8	0.0	3.3	4.6
29	SCA	21	I	0.063	0.064		31.5*	60.8	5.6	33.6	7.8	8.7	18.4	42.8	10.1	0.0	2.0	10.1
30	SCA	21	P	1.415	1.757	5.2	13.7	8.1	4.1	87.9	0.0	0.0	1.5	98.1	0.4	0.0	0.0	0.0
31	SCA	21	R	0.557	1.086	4.4	14.6	8.7	4.2	87.1	0.0	0.0	5.4	93.7	0.8	0.0	0.0	0.0
32	SCA	22	F	0.018	0.021		89.1*	61.9	5.2	33.0	40.0	10.6	3.9	9.7	6.3	0.0	26.5	3.0
33	SCA	22	I	0.003	0.003		n/a*	89.7	6.3	4.1	40.3	11.6	9.5	19.3	8.8	0.0	1.3	9.2
34	SCA	22	P	1.230	0.339	7.0	8.2	34.2	16.3	49.5	0.0	0.0	0.5	98.2	1.3	0.0	0.0	0.0
35	SCA	25	B	0.416	0.286	8.65	24.8	39.0	6.1	54.9	0.0	0.3	18.0	76.7	5.0	0.0	0.0	0.0
36	SCA	25	F	0.336	0.460	5.63	14.8	40.3	8.3	51.8	2.7	7.5	9.6	64.2	6.7	0.2	2.5	6.6
37	SCA	25	I	0.010	0.026			77.4	0.7	21.8	7.2	9.1	17.3	43.0	8.6	1.1	1.2	12.5
38	SCA	25	P	0.357	0.191	4.24	21.9	57.3	6.1	36.6	0.5	3.9	15.7	71.0	5.3	0.0	0.7	3.0
39	SCA	25	P	0.189	0.186	4.65	23.7	18.4	7.2	74.4	6.9	11.1	32.6	31.5	12.2	0.0	5.5	0.1
40	SCA	25	P	0.669	0.354	5.59	22.4	42.3	1.0	56.7	0.0	0.7	37.4	59.5	2.1	0.1	0.2	0.0
41	SCA	25	P	0.311	0.064	5.48	24.9	26.9	9.8	63.3	1.9	7.5	23.4	50.0	4.8	0.0	0.8	11.7
42	SCA	25	P	0.227	0.060	3.10	22.6	29.1	1.1	69.8	2.9	6.3	35.9	42.3	7.7	0.1	2.4	2.3
43	SCA	25	P	0.088	0.046	2.62	25.4	42.7	8.3	49.0	6.3	8.8	33.7	28.3	9.1	0.0	2.2	11.7
44	SCA	25	P	0.949	0.330	7.29	21.8	13.9	7.6	78.5	0.0	0.1	28.6	69.7	1.6	0.0	0.0	0.0
45	SCA	25	P	0.596	0.255	7.00	23.0	13.8	5.1	81.1	0.1	0.1	26.5	71.1	0.7	0.0	0.0	1.5
46	SCA	25	R	0.130	0.110	2.41	17.5	22.1	6.2	71.6	11.5	12.6	24.1	24.9	13.7	0.0	0.8	12.4
47	SCA	25	R	0.132	0.021	4.43	27.7	23.3	6.1	70.6	7.3	8.6	27.9	42.4	6.6	0.0	3.8	3.5
48	SCA	25	R	0.069	0.014	8.14	28.4	52.6	20.0	27.4	8.3	9.6	29.5	34.8	6.9	0.1	3.0	7.9
49	SCA	25	R	0.202	0.218	3.03	22.7	18.3	6.3	75.4	11.3	9.1	27.3	32.2	12.0	0.2	5.4	2.5
50	MCA	15	B	0.145	0.065		22.4	30.3	10.8	58.9	14.9	8.4	11.4	24.2	22.7	0.0	5.5	12.9
51	MCA	15	F	0.028	0.008		64.3*	47.8	23.5	28.8	46.3	3.2	15.0	9.6	4.8	0.0	0.0	21.2
52	MCA	15	I	0.001	0.029		n/a*	73.8	-0.1	26.3	8.7	1.4	0.0	6.6	0.0	0.0	0.5	82.7
53	MCA	15	P	0.470	0.085	4.1	26.8	32.1	7.7	60.2	9.6	6.2	27.6	21.4	11.8	0.0	0.0	23.4
54	MCA	15	R	0.351	0.662	5.1	22.4	19.7	6.2	74.0	8.0	5.4	30.5	40.3	11.7	0.0	1.6	2.5
55	NA	16	B	0.089	0.150		24.1	72.1	5.4	22.5	51.0	7.4	10.4	4.7	4.6	0.0	5.2	16.7
56	NA	16	F	0.073	0.067		40.6	65.0	9.0	26.1	41.8	11.2	25.6	10.8	2.5	0.0	0.6	7.7
57	NA	16	P	0.221	0.267		15.2	68.0	7.1	24.9	27.4	22.4	9.9	14.4	9.4	1.6	7.7	7.1

Table 3 (continued)

Sample No.	Mine Region	No.	Sampling location	PVC sample mass (mg)	TGA recovered mass (mg)	FTIR (mass %)		TGA (mass %)			SEM–EDX (mass %)							
						Q	K	Coal	Carb	Non-carb	C	MC	ASK	ASO	S	SLO	M	CB
58	NA	16	R	0.172	0.253		17.0	62.3	9.7	28.0	53.5	14.0	7.0	9.5	4.4	0.0	3.7	8.0
59	NA	17	B	0.043	0.023		44.8*	46.3	38.1	15.7	7.2	3.0	3.2	16.4	18.0	1.5	5.6	45.0
60	NA	17	I	0.016	0.220		103.2*	93.2	4.1	2.7	2.4	1.4	1.4	3.4	1.8	0.0	1.5	88.1
61	NA	17	I	0.072	0.151		41.6	61.6	6.3	32.1	24.7	5.3	32.9	19.8	4.0	0.0	0.3	13.0
62	NA	17	P	0.277	0.360		29.2	34.9	4.8	60.3	2.5	5.3	42.2	47.1	0.9	0.0	0.4	1.6
63	NA	17	R	0.763	0.826	1.9	24.5	35.4	3.4	61.3	0.0	0.0	59.0	40.3	0.7	0.0	0.0	0.0
64	NA	17	R	0.489	0.713		6.7	30.7	59.0	10.2	14.8	2.4	1.5	6.8	1.0	0.1	0.9	72.5
65	NA	18	B	0.096	0.087		38.0	31.7	9.8	58.5	26.4	5.7	27.2	20.1	8.3	0.1	4.2	7.9
66	NA	18	F	0.018	0.025		n/a	71.3	6.4	22.3	24.1	5.4	16.2	17.4	4.3	0.5	1.4	30.7
67	NA	18	I	0.002	0.018		n/a*	67.7	12.2	20.1	7.9	1.8	4.0	3.8	1.2	0.0	1.1	80.0
68	NA	18	P	0.340	0.095		25.0	39.5	5.7	54.9	1.0	1.4	38.2	54.5	2.8	0.0	0.0	2.1
69	NA	18	R	0.231	0.113		26.1	41.5	7.7	50.8	21.7	10.5	34.5	25.3	6.8	0.1	0.0	1.1
70	MW	19	B	0.181	0.071		17.2	56.9	9.0	34.1	8.0	21.3	1.4	48.7	7.7	0.0	0.7	12.2
71	MW	19	F	2.608	0.901	4.6	8.8	48.4	6.1	45.5	0.4	1.6	3.8	82.2	10.6	0.2	0.4	0.8
72	MW	19	I	0.014	0.006		86.7*	0.0	48.8	51.3	15.7	13.9	2.5	24.4	4.8	0.8	1.6	36.3
73	MW	19	P	0.277	0.333		9.5	49.5	16.7	33.8	13.6	11.6	0.0	32.4	3.5	0.2	5.8	32.8
74	MW	19	R	0.299	0.319		8.4	45.2	20.6	34.2	9.8	19.9	0.1	37.8	4.2	0.5	2.8	25.0
75	MW	19	R	0.223	0.291		12.8	47.2	5.0	47.8	13.8	19.6	8.0	48.8	5.1	0.2	1.7	2.9
76	MW	20	B	0.530	0.413		10.7	32.0	21.4	46.6	0.0	1.5	0.1	68.1	1.0	0.0	0.7	28.6
77	MW	20	F	0.143	0.024		15.2	32.1	35.9	32.0	27.3	6.0	1.6	16.6	7.8	0.0	2.4	38.4
78	MW	20	F	0.191	0.130		12.8	36.6	21.2	42.2	19.4	10.7	3.5	28.2	6.0	0.1	0.1	32.1
79	MW	20	I	0.019	0.041		62.6*	57.5	28.3	14.1	16.8	7.5	0.5	2.6	3.8	0.6	3.4	64.7
80	MW	20	P	0.758	0.613	0.5*	10.3	31.4	8.6	60.0	0.0	0.0	0.2	94.8	0.6	0.0	0.0	4.3
81	MW	20	R	0.577	0.317		11.1	32.7	11.1	56.2	7.7	19.6	2.9	45.4	2.8	0.0	1.3	20.2
82	W	23	I	n/a	0.231	n/a	n/a*	67.8	18.0	14.3	65.9	3.9	1.5	1.2	4.2	0.0	5.8	17.5
83	W	23	I	0.097	0.051		12.2*	30.6	58.7	10.6	6.3	1.3	0.0	2.2	0.0	0.0	0.0	90.3
84	W	23	I	0.176	0.164		9.5*	40.8	50.7	8.5	15.3	4.3	0.0	1.3	0.8	0.1	0.5	77.7
85	W	23	P	0.349	0.351		4.4*	5.8	68.0	26.2	1.4	0.9	0.0	0.2	0.1	0.0	0.1	97.3
86	W	23	P	0.268	0.215		4.7*	n/a	n/a	n/a	n/a	n/a	n/a	n/a	n/a	n/a	n/a	n/a
87	W	23	R	0.888	1.061		4.7	29.0	62.1	8.9	1.3	1.8	0.0	0.6	0.1	0.0	0.0	96.2
88	W	24	F	0.068	0.134		26*	70.9	9.8	19.3	37.0	7.1	0.2	10.7	5.5	0.2	0.1	39.1
89	W	24	I	1.547	1.492	24.9	7.5	30.7	2.9	66.4	0.6	1.3	0.0	3.0	94.6	0.4	0.0	0.0
90	W	24	I	0.052	0.051		24.1*	68.2	15.9	15.9	27.8	7.8	2.0	10.1	4.7	1.2	0.3	46.1
91	W	24	I	0.063	0.064		27.5*	53.0	20.0	27.0	23.6	2.8	0.0	7.5	4.0	1.7	2.3	58.1
92	W	24	R	0.165	0.195		13.5	43.7	14.0	42.3	14.6	7.8	0.4	19.5	20.4	1.8	0.0	35.5
93	W	24	R	5.361	5.312	3.5	3.7	12.3	70.2	17.6	0.3	0.2	0.0	5.7	0.0	0.9	0.0	93.0

*samples between LOD and LOQ.

n/a*: data unavailable (these samples are between LOD and LOQ, and have very low/missing sample mass).

n/a: data unavailable.

empty cells: samples below LOD.

3.1 Comparison of mass-based FTIR and TGA

Comparison of FTIR (Q + K) % with TGA estimation of non-carbonates % is shown in Fig. 1. The results are plotted as the difference between the two measures as a function of sample mass. There is a clear transition in the data around 100 μg, which is attributed to decreased analytical accuracy with lower sample mass. As noted, most of the low-mass samples in this study were collected in I, B, and F locations. For higher-mass samples, the tendency of the TGA result to be significantly higher than the FTIR result indicates that quartz and kaolinite do not account for all of the non-carbonate mineral content in most of these respirable dust samples. Indeed, the SEM–EDX results (Table 3) show relatively high abundance of non-kaolinite aluminosilicates (i.e., ASO) in many of the samples, which could be feldspars, micas, etc. Further analysis of both the SEM–EDX elemental data and the FTIR spectra—in terms of potential peaks related to other silicates/minerals along with potential interferences—could provide useful insights on this topic and will be the focus of future work.
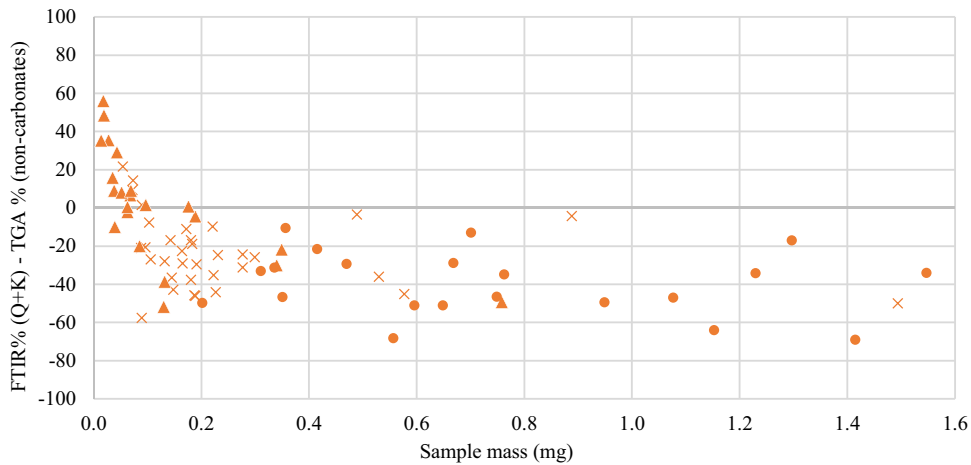
Fig. 1 Difference between FTIR-based (Q + K) % and TGA-based non-carbonate mineral mass % versus dust mass on each PVC replicate (n = 83). In 33 out of 93 samples, Q was below LOD, but K was above LOQ. The x-axis is capped at 1.6 mg since most of the data points are clustered in this range; 5 more data points exist between 1.6—8 mg, all following the observed trend. ✕ = either Q or K below LOD, ▲ = either Q or K between LOD and LOQ; ● = both K and Q above LOQ. (Updated from [26].)

Fig. 2 Difference between FTIR- and SEM–EDX-derived mass % estimates for quartz/silica and kaolinite/aluminosilicates-kaolinite versus dust mass on each PVC replicate (n = 33 for Q%-S%, n = 83 for K%-ASK%). The x-axis is capped at 1.6 mg; 10 more data points exist (5 each for Q and K) between 1.6 and 8 mg, all following the observed trend. ✕ = below LOD, ▲ = between LOD and LOQ; ● = above LOQ. (Updated from [26].)
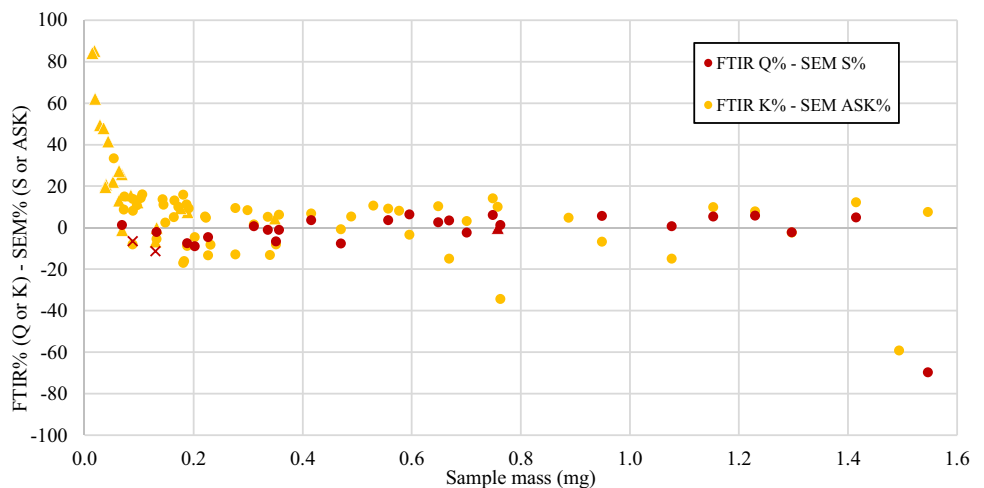
3.2 Comparison of FTIR and TGA to particle-based SEM–EDX

Figure 2 shows the comparison between the FTIR and SEM–EDX results. As expected, results for FTIR-derived Q and SEM–EDX-derived S are in reasonable agreement (i.e., mean difference of about ± 5%, apart from one outlier). That said, all but the outlier sample had < 25% Q/S per either method, so the visual similarities between the two data series (Fig. 2) should be viewed accordingly.

Similar to the Q/S results, Fig. 2 shows that FTIR-derived K and SEM–EDX-derived ASK results generally agree (mean difference of about ± 15%). Since the K/ASK

abundance ranged from 0% up to about 90% per either method, a mean difference of ± 15% can be considered to represent a good agreement. Like for the comparison between FTIR and TGA shown in Fig. 1, trends with sample mass are evident in Fig. 2, with the lowest-mass samples likely being affected by accuracy issues. Considering there is a reasonable agreement in K/ASK% across most of the mass range and ASK % is, on average, one-fourth of the total AS (i.e., ASK + ASO) per Table 3, it can be inferred there is indeed an abundance of non-kaolinite aluminosilicates in many of the samples.

Figure 3 shows the comparison between the TGA and SEM–EDX results. In this case, all three primary

Fig. 3 Difference between estimates of coal, carbonates, and non-carbonate mineral fractions derived from TGA and SEM–EDX results versus dust mass collected on each PVC replicate (n = 91). The x-axis is capped at 1.6 mg; 5 sets of data points exist between 1.6 and 8 mg, all roughly following the observed trend. (Updated from [26].)
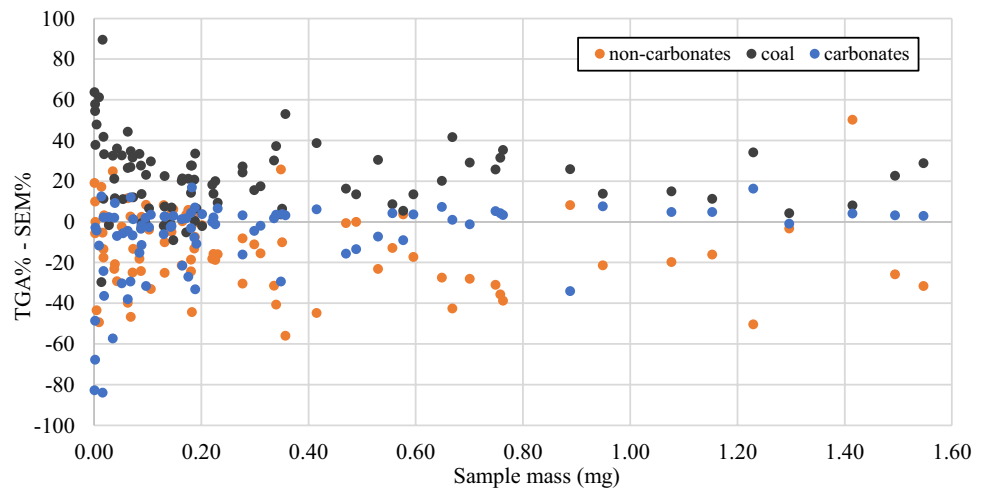
components of the dust estimated by TGA (i.e., coal, carbonate, and non-carbonates) can be compared with results from SEM–EDX since its mineralogy classes can be collapsed to roughly match the TGA outputs per Table 1. The largest differences are again seen for the lowest-mass samples. Figure 3 suggests that these discrepancies are most often related to a tendency for the TGA to measure more coal (possibly including very fine diesel particulates not accurately counted in the SEM–EDX work) and less carbonate (possibly overcounted in the SEM–EDX work due to its coarser size, see [22].

The effect of sample mass in Fig. 3 is visibly diminished above about 100 μg. Above that threshold, in general, the SEM–EDX still tends to overpredict non-carbonate minerals (mostly ASK + ASO + S per Table 3) versus the TGA. Frequently, this overprediction of non-carbonates by the SEM–EDX corresponds with an underprediction of coal (C + MC), especially for samples collected nearby to activities that generate very fine dust (i.e., production, roof bolting, and in the return). Possible explanations for these results could be that coal particles are either impure or are otherwise being classified as minerals (e.g., due to fine aluminosilicates sitting on or nearby to coal dust). Since the SEM–EDX classifies particles into discrete bins based on their elemental content (Table 2), classification of particles as minerals that are actually mostly coal by mass could lead to substantial discrepancies between particle- and mass-based results. Notably, the fact that the carbonate results in Fig. 3 (like the Q/S results in Fig. 2) are in relatively good agreement provides some indication that high sample mass is probably not the only reason for high ASK + ASO content per SEM–EDX—meaning, particle interference effects due to sample loading are not alone responsible.

3.3 Results by sampling location and mine region

Figure 4 presents the FTIR, TGA, and SEM–EDX results grouped by sampling location (I, B, F, P, and R) and split between mines in central Appalachia (regions SCA and MCA per Table 3) those outside central Appalachia (regions NA, MW, and W). It is noted that, to construct this plot, samples with < 100 μg respirable dust mass on the PVC filter were excluded based on observations in Figs. 1, 2, and 3. This yielded just three I samples across the entire dataset, and few B and F samples to represent the mines outside of central Appalachia—so results should be viewed accordingly. Nevertheless, Fig. 4 suggests that the relative agreement (or disagreement) between the three analytical methods is generally consistent across sampling locations and regions. This includes the tendency for the SEM–EDX to overpredict total non-carbonate minerals (mostly S + ASK + ASO) and underpredict coal (C + MC), and relative to the TGA. That tendency appears more pronounced in samples from central Appalachian mines. In samples from other mines, underprediction of the coal by the SEM–EDX is also balanced by a slight overprediction of carbonates (CB), which might be related to particle size effects (i.e., the SEM–EDX analysis is done in a limited size range and coal and carbonate size distributions may vary by region). Overall, agreement among all three methods appears to be best for samples collected in the R location, though no clear explanation has been elucidated.

Regarding the relative abundance of dust constituents by sampling location and region, Fig. 4 also shows that rock-strata sourced dust (i.e., non-carbonate minerals including quartz) was generally more abundant in the central Appalachian mine samples. This is consistent with previous findings where either TGA or SEM–EDX was used to analyze respirable dust from other central

Fig. 4 Mean mass % of respirable coal mine dust constituents determined by FTIR, TGA, and SEM–EDX in samples with > 100 μg PVC sample mass per Table 3. Results are grouped by sampling location and split between central Appalachia and mines outside central Appalachia (regions NA, MW, W); n values indicate number of samples in each group
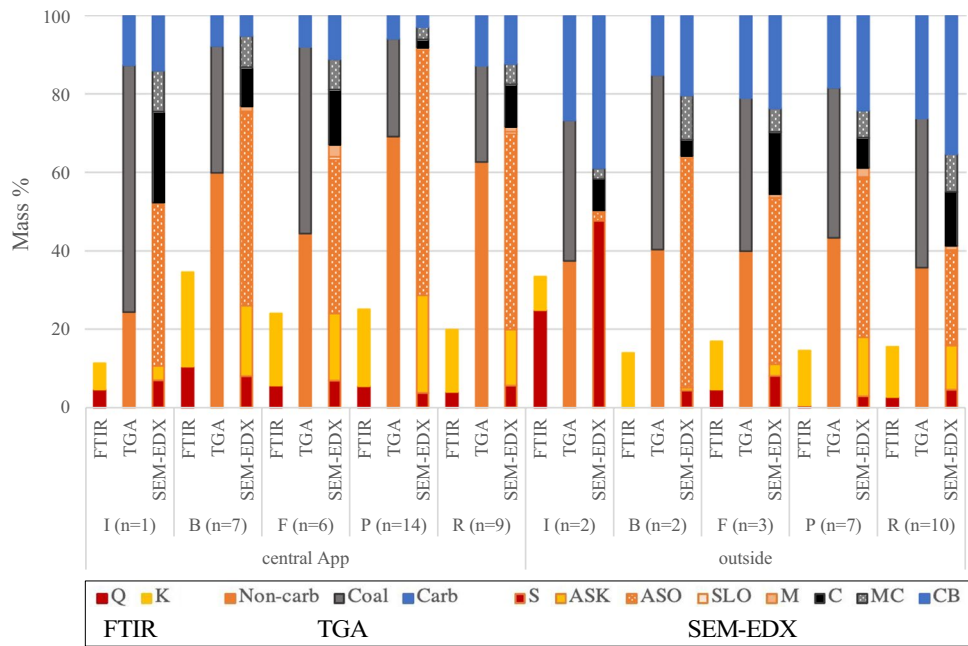
Appalachian mines [21, 27, 28], and with expectations based on thin-seam mining practices in the region. In the current study, the rock strata accounted for an average of about 44% of the total mining height in the central Appalachian mines (during dust sampling), whereas it was only about 16% for the other mines. It is also worth noting that rock dust application was generally more evident in the mines outside of central Appalachia, which explains the relatively higher abundance of carbonate content in dust samples from these mines.

4 Conclusions

This study investigated mineral content in respirable coal mine dust samples derived from three analytical methods: DOF-FTIR, TGA, and SEM–EDX. Overall, results suggest the presence of significant non-carbonate mineral content other than quartz and kaolinite in the dust from many mines. Detailed analysis of the FTIR transmission and SEM–EDX elemental spectra might be valuable to better understand the specific mineral constituents. Further, results showed that the particle-based SEM–EDX frequently indicates much more mineral content (primarily aluminosilicates other than kaolinite) and less coal than is predicted by the mass-based TGA; this is in spite of better agreement for carbonates as well as reasonable agreement between SEM–EDX and FTIR for silica/quartz and kaolinite. While sample mass/particle loading effects may be

partly to blame, another possibility is that the SEM–EDX results are influenced by agglomeration of fine aluminosilicates with coal.

Aside from enabling direct comparison of results between the three analytical methods, this study represents one of the first applications of the DOF-FTIR method for research purposes. While this method has been developed with the primary intention of "end-of-shift" silica monitoring, application here clearly illustrates its broader usefulness for research and engineering studies. In addition to quartz, reasonable estimation of kaolinite is possible—and other recent work by the authors has also demonstrated the utility of the DOF-FTIR method for estimating calcite as a proxy for limestone rock dust in respirable coal mine dust samples (see [17]).

Of course, the selection of an appropriate analytical method must consider a wide range of factors, including the level of detail and accuracy required for data, and the time and costs associated with acquiring that data. For mine operators seeking relatively quick and inexpensive silica monitoring, with the added benefit of tracking kaolinite and calcite as proxies for major dust sources, the DOF-FTIR method appears favorable. On the other hand, for the additional time and costs, laboratory-based methods such as SEM–EDX can afford additional insights (e.g., particle size, other minerals). In any case, sampling protocols should be tailored to the planned analysis (e.g., to achieve appropriate dust loading and minimize the need for sample handling prior to analysis).

Declarations

Conflict Of Interest We declare no conflicts of interest.

References

1. IARC (1997) Monographs on the evaluation of carcinogenic risks to humans: silica, some silicates, coal dust and para-aramid fibrils., Lyon, France.

2. NASEM (2018) Monitoring and Sampling Approaches to Assess Underground Coal Mine Dust Exposures. DC, The National Academies Press, Washington

3. Castranova V, Vallyathan V (2000) Silicosis and coal workers' pneumoconiosis. Environ Health Perspect 108(Suppl 4):675–684

4. Laney AS, Weissman DN (2014) Respiratory diseases caused by coal mine dust. J Occup Environ Med 56(Suppl 10):S18-22

5. Schatzel SJ (2009) Identifying sources of respirable quartz and silica dust in underground coal mines in southern West Virginia, western Virginia, and eastern Kentucky. Int J Coal Geol 78:110–118

6. Almberg KS, Halldin CN, Blackley DJ, Laney AS, Storey E, Rose CS, Go LHT, Cohen RA (2018) Progressive Massive Fibrosis Resurgence Identified in U.S. Coal Miners Filing for Black Lung Benefits, 1970–2016. Ann Am Thorac Soc 15:1420–1426

7. BLACKLEY, D. J., CRUM, J. B., HALLDIN, C. N., STOREY, E. & LANEY, A. S. (2016) Resurgence of Progressive Massive Fibrosis in Coal Miners. Morbidity and Mortality Weekly Report.

8. CDC (2006) Advanced Cases of Coal Workers' Pneumoconiosis --- Two Counties, Virginia. MMWR 55.

9. Ashley EL, Cauda E, Chubb LG, Tuchman DP, Rubinstein EN (2020) Performance Comparison of Four Portable FTIR Instruments for Direct-on-Filter Measurement of Respirable Crystalline Silica. Ann Work Expo Health 64:536–546

10. Cauda E, Miller A, Drake P (2016) Promoting early exposure monitoring for respirable crystalline silica: Taking the laboratory to the mine site. J Occup Environ Hyg 13:D39-45

11. Miller AL, Drake PL, Murphy NC, Cauda EG, Lebouf RF, Markevicius G (2013) Deposition Uniformity of Coal Dust on Filters and Its Effect on the Accuracy of FTIR Analyses for Silica. Aerosol Sci Technol 47:724–733

12. MSHA (2008) Method No. P-7. Pittsburgh Safety and Health Technology Center.

13. Miller AL, Drake PL, Murphy NC, Noll JD, Volkwein JC (2012) Evaluating portable infrared spectrometers for measuring the silica content of coal dust. J Environ Monit 14:48–55

14. Miller AL, Weakley AT, Griffiths PR, Cauda EG, Bayman S (2017) Direct-on-Filter alpha-Quartz Estimation in Respirable Coal Mine Dust Using Transmission Fourier Transform Infrared Spectrometry and Partial Least Squares Regression. Appl Spectrosc 71:1014–1024

15. Su X, Ding R, Zhuang X (2020) Characteristics of Dust in Coal Mines in Central North China and Its Research Significance. ACS Omega 5:9233–9250

16. Lee T, Chisholm WP, Kashon M, Key-Schwartz RJ, Harper M (2013) Consideration of kaolinite interference correction for quartz measurements in coal mine dust. J Occup Environ Hyg 10:425–434

17. Pokhrel N, Keles C, Jaramillo L, Agioutanti E, Sarver E (2021) Direct-on-Filter FTIR Spectroscopy to Estimate Calcite as a Proxy for Limestone 'Rock Dust' in Respirable Coal Mine Dust Samples. Min 11:922

18. Stach R, Barone T, Cauda E, Krebs P, Pejcic B, Daboss S, Mizaikoff B (2020) Direct infrared spectroscopy for the size-independent identification and quantification of respirable particles relative mass in mine dusts. Anal Bioanal Chem 412:3499–3508

19. Agioutanti E, Keles C, Sarver E (2020) A thermogravimetric analysis application to determine coal, carbonate, and non-carbonate minerals mass fractions in respirable mine dust. J Occup Environ Hyg 17:47–58

20. Johann-Essex V, Keles C, Sarver E (2017) A Computer-Controlled SEM-EDX Routine for Characterizing Respirable Coal Mine Dust. Minerals 7:15

21. Sarver E, Keleş Ç and Afrouz SG (2021) Particle size and mineralogy distributions in respirable dust samples from 25 US underground coal mines. Int J Coal Geol, 247.

22. Sarver E, Keles C, Rezaee M (2019) Beyond conventional metrics: Comprehensive characterization of respirable coal mine dust. Int J Coal Geol 207:84–95

23. Johann-Essex V, Keles C, Rezaee M, Scaggs-Witte M, Sarver E (2017) Respirable coal mine dust characteristics in samples collected in central and northern Appalachia. Int J Coal Geol 182:85–93

24. Chubb LG, Cauda EG (2021) A novel sampling cassette for field-based analysis of respirable crystalline silica. J Occup Environ Hyg 18:103–109

25. NIOSH (2019) FAST (Field Analysis of Silica Tool). Build 1.0.7.2 ed. Pittsburgh, PA, NIOSH-CDC.

26. Pokhrel N, Agioutanti E, Keles C, Afrouz S and Sarver E. (2021) Comparison of mineral content in respirable coal mine dust samples estimated using FTIR, TGA, and SEM-EDX. 18th North American Mine Ventilation Symposium.

27. Phillips K, Keles C, Scaggs-Witte M, Johann-Essex V, Rezaee M, Sarver E (2017) Applications of thermal and laser-based methods for monitoring airborne particulates in coal mines. Blacksburg, VA, Virginia Polytechnic Institute and State University, Department of Mining and Minerals Engineering

28. Phillips K, Keles C, Scaggs-Witte M, Sarver E (2018) Coal and mineral mass fractions in personal respirable dust samples collected by central appalachian miners. Min Eng 70:16

Publisher's Note Springer Nature remains neutral with regard to jurisdictional claims in published maps and institutional affiliations.